JOURNAL OF Materials CHEMISTRY

Spectral, magnetic and electrochemical studies of layered manganese oxides with P2 and O2 structure

K. M. Shaju,[a] K. V. Ramanujachary,[b] S. E. Lofland,[b] G. V. Subba Rao[a] and B. V. R. Chowdari*[a]

[a]*Department of Physics, National University of Singapore, Singapore 119260*
[b]*Department of Physics and Chemistry, Rowan University, New Jersey 08028-1701, USA*

Received 27th January 2003, Accepted 22nd July 2003
First published as an Advance Article on the web 28th August 2003

X-Ray photoelectron spectroscopy (XPS), infrared spectroscopy and magnetic susceptibility studies were performed on layered O2-phase compounds, $Li_{2/3}(Ni_{1/3}Mn_{2/3})O_2$, $Li_{(2/3)+x}(Ni_{1/3}Mn_{2/3})O_2$, $Li_{2/3}(Co_{0.15}Mn_{0.85})O_2$ and $Li_{(2/3)+x}(Co_{0.15}Mn_{0.85})O_2$ and their respective P2 phases, $Na_{2/3}(Ni_{1/3}Mn_{2/3})O_2$ and $Na_{2/3}(Co_{0.15}Mn_{0.85})O_2$. The observed electrochemical performance was correlated with the oxidation states of the M ions (M = Mn, Ni, Co). $Li_{(2/3)+x}(Ni_{1/3}Mn_{2/3})O_2$ and $Li_{(2/3)+x}(Co_{0.15}Mn_{0.85})O_2$ show significant improvement in their first-charge capacity over $Li_{2/3}(Ni_{1/3}Mn_{2/3})O_2$ and $Li_{2/3}(Co_{0.15}Mn_{0.85})O_2$ when used as cathodes *vs.* Li. Chemical analysis and XPS data indicate that the incorporation of $x \sim \frac{1}{3}$ in the above two compounds is accompanied by the reduction of a corresponding amount of Mn^{4+} to Mn^{3+} ions in the lattice. The magnetic moments obtained in the paramagnetic region are in fair agreement with the oxidation state of the ions derived from the XPS data for the Ni-system but show deviations for the Co-system. Below 100 K, weak ferrimagnetic ordering is observed in $Li_{(2/3)+x}(Ni_{1/3}Mn_{2/3})O_2$ and $Li_{(2/3)+x}(Co_{0.15}Mn_{0.85})O_2$.

1 Introduction

Mixed manganese oxides $A_x(M_yMn_{1-y})O_2$ (M = Co, Ni, Li; A = Na, Li; $x \leqslant 1$; y = 0–1.0) are of interest as positive electrodes in Li-ion batteries (LIB). They can adopt different types of layered structure, the so called P2, P3, T2, O2 and O3 structures. The terminology is based on the metal–oxygen stacking sequence and the oxygen coordination of the A ion (P: trigonal prismatic, T: tetrahedral and O: octahedral) and by the number of $(M,Mn)O_2$ sheets (2 or 3) per unit cell.[1–4] The [110] projections of some of the above structures are shown in Fig. 1. As can be seen, each MO_2 layer in the O2-phase is mirrored and its oxygen stacking sequence necessitates breaking and rearrangement of M–O (M = Ni, Co, Mn) bonds to convert it to the O3 or spinel structure. Thus O2→O3 conversion does not occur under 'soft' chemistry or electrochemical charge–discharge cycling. The oxide cathode, $LiCo^{3+}O_2$ used in the LIB and $LiNi^{3+}O_2$ and its derivatives, $Li(Ni_{1-x}M_x)O_2$ (M = Co, Cr, Mn) are O3-type.[5–9] The O3 structure is rhombohedral–hexagonal (α-$NaFeO_2$ type) with ordered Li and M layers

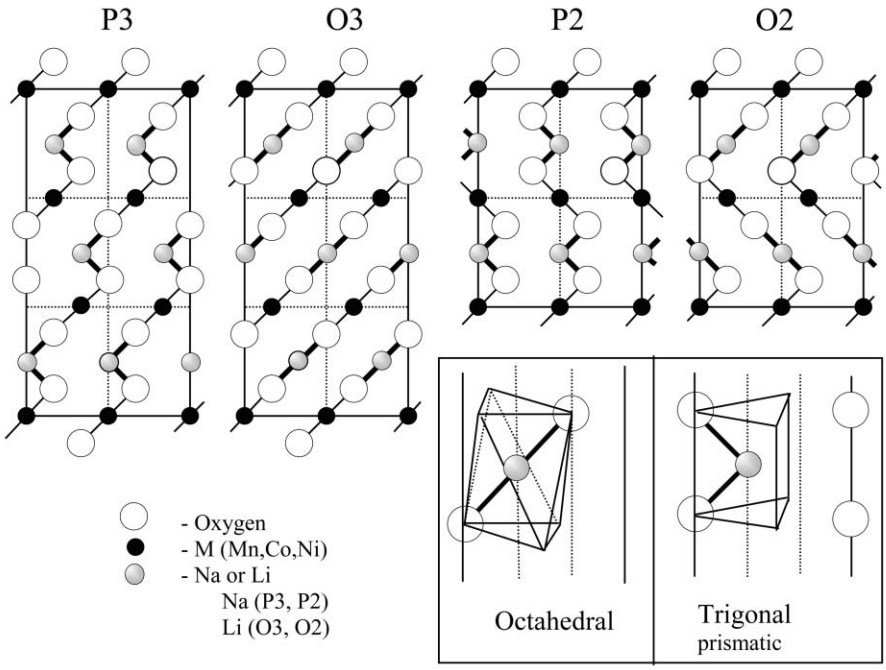

Fig. 1 Layered structures consisting of rigid MO_2 sheets viewed along the [110] direction. M = a transition metal in octahedral coordination. P: trigonal prismatic coordination (adopted by Na), O: octahedral coordination (adopted by Li). The numbers (3 or 2) refer to the MO_2 layers per unit cell. Thick lines enclose two unit cells in each case. Schematic of projection of P and O coordination are also shown. Note that MO_2 layers in P3 and O3 have the same orientation although this is not the case with P2 and O2 structures.

in a fcc close-packed oxygen lattice. It is related to the spinel structure ($LiMn_2O_4$) in which Li and Mn ions respectively occupy the tetrahedral and octahedral holes in an fcc oxygen lattice. The O3 $LiMn^{3+}O_2$ transforms to $LiMn_2O_4$ ($Li_{0.5}MnO_2$) during the charging operation as the cathode, where the Li ions move from octahedral oxygen to tetrahedral coordination.[10–12]

The O2 $Li_{2/3}(M_yMn_{1-y})O_2$ (M = Co, Ni, Li; $y = \frac{1}{6}$–$\frac{2}{3}$) compounds have been recently studied by Dahn and his co-workers[3,4,13–16] as prospective cathodes for LIB. The O2 compounds are obtained by Na to Li ion exchange of the corresponding P2 phases, $Na_{2/3}(M_yMn_{1-y})O_2$, which can be prepared by a high-temperature solid-state reaction. The P2-to-O2 (and P3-to-O3) structure conversion involves only minor sliding of the MO_2 sheets with respect to one another in the layer structure (Fig. 1) and occurs during the ion-exchange process. The O2-phase compounds, $Li_{2/3}(Ni_{1/3}Mn_{2/3})O_2$ and $Li_{2/3}(Co_{0.15}Mn_{0.85})O_2$, have received more attention due to their easy synthesis and interesting electrochemical behaviour.

We have incorporated extra lithium ($x = \frac{1}{3}$) to obtain O2 $Li_{(2/3)+x}(Ni_{1/3}Mn_{2/3})O_2$[17,18] and $Li_{(2/3)+x}(Co_{0.15}Mn_{0.85})O_2$[19,20] using LiI during the ion-exchange process. Electrochemical studies have shown that they have a high first-charge capacity together with reversible and stable cycling performance as cathodes *vs.* the Li anode at ambient temperature (25 °C) and at 50 °C.[17–20] Here, we report the physical properties of these oxide cathodes and make correlations with the observed electrochemical behaviour.

2 Experimental

The precursor compounds, $Na_{2/3}(Ni_{1/3}Mn_{2/3})O_2$ and $Na_{2/3}(Co_{0.15}Mn_{0.85})O_2$, were synthesized by high-temperature (900–1000 °C) solid-state reactions as described elsewhere.[3,4,17–20] Stoichiometric amounts of high purity (Alfa, USA) alkali carbonates, NiO/Co_3O_4 and Mn_2O_3 powders were used. Ion exchange of sodium (Na) for lithium (Li) was done using a melt of a eutectic mixture of $LiNO_3$ and LiCl (88 : 12 mol%) at 280 °C. Incorporation of extra lithium was carried out during the ion-exchange process by the addition of LiI (Alfa) to the eutectic melt with a fresh batch of the precursors as reported elsewhere.[17,19] The compounds were characterized by powder X-ray diffraction (Siemens D5005; Cu-Kα radiation).

Chemical analysis for Na, Li, Ni, Co and Mn in the compounds was done by inductively coupled plasma spectroscopic analysis. The infrared (IR) spectra in the range 400–4000 cm^{-1} were recorded with a Bruker Equinox 55 Fourier-transform infrared (FTIR) spectrometer. Samples were mixed with KBr and pressed to form translucent pellets for measurement. X-Ray photoelectron spectra (XPS) were obtained with a VG Scientific ESCA MK II spectrometer with monochromatic Mg-Kα radiation ($h\nu$ = 1253.6 eV). The survey spectra in the range 0–1099 eV (constant-pass energy = 50 eV) and high-resolution spectra (constant-pass energy = 20 eV) were recorded. Charge referencing was made against the binding energy (BE) of adventitious carbon (C 1s = 284.6 eV). The spectra were analyzed with the XPS peak fit software. A Shirley-type background was subtracted from the recorded spectra and curve fitting of the peaks was done by non-linear least-squares fitting with a Gaussian–Lorentzian (ratio 60 : 40) curve. The BEs are accurate to ±0.1 eV. The magnetic susceptibility studies were performed on powders in the range 5 K < T < 300 K with a Physical Property Measurement System (Quantum Design, USA) at a field of 0.1 Tesla. Field-dependent magnetization measurements on selected samples were done at 5 K in fields of up to 9 Tesla. For the electrochemical measurements, coin cells (size, 2016) were assembled in an argon-filled glove box at <1 ppm of H_2O and O_2 (MBraun, Germany), with 1 M $LiPF_6$ in ethylene carbonate (EC)–diethyl carbonate (DEC) (1 : 1 volume, Merck, Selectipur LP40) as the electrolyte and a Celgard 2502 membrane as separator. Li-metal foil (Kyokuto Metal Co., Japan) was used as the anode. Details of fabrication have been described elsewhere.[17,19] Charge–discharge cycling and cyclic voltammetry tests at ambient temperature were carried out with a potentiostat/galvanostat system (Mac-pile II, Bio-logic, France) and Bitrode multiple battery tester (Model SCN, Bitrode, USA).

3 Results and discussion

3.1 Composition and structure

The precursor compounds, $Na_{2/3}(Co_{0.15}Mn_{0.85})O_2$, $Na_{2/3}(Ni_{1/3}Mn_{2/3})O_2$ and their Li-ion-exchanged counterparts, $Li_{2/3}(Co_{0.15}Mn_{0.85})O_2$, $Li_{2/3}(Ni_{1/3}Mn_{2/3})O_2$ are black whereas the respective excess Li-incorporated compounds, $Li_{(2/3)+x}(Co_{0.15}Mn_{0.85})O_2$ and $Li_{(2/3)+x}(Ni_{1/3}Mn_{2/3})O_2$ are light brown in color and are stable in air. The X-ray diffraction results for the compounds $Na_{2/3}(Co_{0.15}Mn_{0.85})O_2$, $Li_{2/3}(Co_{0.15}Mn_{0.85})O_2$ and $Li_{(2/3)+x}(Co_{0.15}Mn_{0.85})O_2$ revealed that the Na-to-Li ion exchange was incomplete and a small fraction (3–5%) of the parent phase remained in both $Li_{2/3}(Co_{0.15}Mn_{0.85})O_2$ and $Li_{(2/3)+x}(Co_{0.15}Mn_{0.85})O_2$.[19] Paulsen *et al.*[3] also reported similar behavior for $Li_{2/3}(Co_{0.15}Mn_{0.85})O_2$. The $Li_{2/3}(Co_{0.15}Mn_{0.85})O_2$ and $Li_{(2/3)+x}(Co_{0.15}Mn_{0.85})O_2$ phases adopt the O2-structure with hexagonal symmetry.[19] Complete Na-to-Li ion exchange was observed in $Li_{2/3}(Ni_{1/3}Mn_{2/3})O_2$ and $Li_{(2/3)+x}(Ni_{1/3}Mn_{2/3})O_2$ with the latter compounds crystallizing in the orthorhombic T2-structure.[4,13,17,18] Chemical analysis results for the compounds were in agreement with expected stoichiometry taking into account a ±5–8% uncertainty in determining the Na and Li content, and a ±2–4% uncertainty in the analysis of Ni, Mn and Co. Oxygen content was not analyzed and was assumed to be 2.0. Chemical analysis also confirmed that the Li content is close to 1.0 ($x \sim \frac{1}{3}$) in $Li_{(2/3)+x}(Ni_{1/3}Mn_{2/3})O_2$ and

Table 1 Chemical formula, XPS binding energies (±0.1 eV) and magnetic parameters of the oxide cathodes

	XPS binding energies/eV											
	Mn $2p_{3/2}$		Ni $2p_{3/2}$		Co $2p_{3/2}$	Mn 3p				Weiss temperature,	Measured moment,	Calculated moment [a]
Compound formula	Mn^{3+}	Mn^{4+}	Ni^{2+}	Ni^{3+}	Co^{3+}	Mn^{3+}	Mn^{4+}	Li 1s	O 1s	θ/K	$\mu_{eff(exp)}/\mu_B$	$\mu_{eff(cal)}/\mu_B$
$Na_{2/3}(Ni^{2+}_{1/3}Mn^{4+}_{2/3})O_2$	641.3	642.3	854.2	856.1	—	—	—	—	529.0, 530.8	−58	3.38	3.56, (3.63)
$Li_{2/3}(Ni^{2+}_{1/3}Mn^{4+}_{2/3})O_2$	641.5	642.4	854.5	856.4	—	49.1	49.7	54.1	529.3, 531.2	−107	3.66	3.56, (3.63)
$Li_{1.0}(Ni^{2+}_{1/3}Mn^{3+}_{1/3}Mn^{4+}_{1/3})O_2$	641.8	643.1	854.4	856.1	—	49.4	50.0	54.3	529.3, 531.1	−62	3.64	3.96, (3.97)
$Na_{2/3}(Co^{3+}_{0.15}Mn^{3+}_{0.52}Mn^{4+}_{0.33})O_2$	641.7	643.5	—	—	779.9	—	—	—	529.3, 530.8	−140	3.32	4.18
$Li_{2/3}(Co^{3+}_{0.15}Mn^{3+}_{0.52}Mn^{4+}_{0.33})O_2$	641.9	643.2	—	—	780.2	49.8	50.8	54.1	529.4, 531.1	−98	3.61	4.18
$Li_{1.0}(Co^{3+}_{0.15}Mn^{3+}_{0.85})O_2$	642.1	—	—	—	780.0	49.8	—	54.1	529.4, 531.3	−154	4.11	4.52

[a]Assuming low-spin configuration for Ni^{3+} and Co^{3+} ions. Values in brackets are calculated as per ion equilibrium (see text).

$Li_{(2/3)+x}(Co_{0.15}Mn_{0.85})O_2$, in agreement with the formula given in Table 1.

3.2 Electrochemical performance

The electrochemical performances and Li-ion kinetics of the compounds $Li_{2/3}(Ni_{1/3}Mn_{2/3})O_2$ and $Li_{(2/3)+x}(Ni_{1/3}Mn_{2/3})O_2$,[17,18] $Li_{2/3}(Co_{0.15}Mn_{0.85})O_2$ and $Li_{(2/3)+x}(Co_{0.15}Mn_{0.85})O_2$[19,20] have been discussed in detail elsewhere. As mentioned therein, $Li_{(2/3)+x}(Ni_{1/3}Mn_{2/3})O_2$ and $Li_{(2/3)+x}(Co_{0.15}Mn_{0.85})O_2$ were found to have enhanced first-extraction capacity thereby making them suitable as cathodes in LIB. Studies on $Li_{2/3}(Ni_{1/3}Mn_{2/3})O_2$ and $Li_{2/3}(Co_{0.15}Mn_{0.85})O_2$ revealed that extra Li incorporation also occurs by electrochemical means during the first-discharge process.[3,4,13,17–20] The process is accompanied by the reduction of a corresponding amount of Mn^{4+} to Mn^{3+} ions in the compounds. The first-extraction capacity of $Li_{(2/3)+x}(Ni_{1/3}Mn_{2/3})O_2$ (190 mA h g^{-1}) is nearly a two-fold improvement over that of $Li_{2/3}(Ni_{1/3}Mn_{2/3})O_2$ (108 mA h g^{-1}) as shown in Fig. 2a. This is due to the fact that only ⅙ of Ni^{2+} can be oxidized to Ni^{4+} in $Li_{2/3}(Ni_{1/3}Mn_{2/3})O_2$ and Mn^{4+} ions are inactive above 4.0 V *vs.* Li, whereas in the case of $Li_{(2/3)+x}(Ni_{1/3}Mn_{2/3})O_2$ an additional $\frac{1}{3}$ mole extraction of Li is possible due to the oxidation of Mn^{3+} in the lattice. The reversible capacity and capacity retention of $Li_{(2/3)+x}(Ni_{1/3}Mn_{2/3})O_2$ on cycling at 25 °C and 50 °C (at 15 mA g^{-1}; 2.5–4.6 V) was shown to be much better than that of $Li_{2/3}(Ni_{1/3}Mn_{2/3})O_2$.[17,18] Further, qualitative change in the charge–discharge profile was noticed in $Li_{(2/3)+x}(Ni_{1/3}Mn_{2/3})O_2$ which delivers its total cathodic capacity mostly above 3 V whereas $Li_{2/3}(Ni_{1/3}Mn_{2/3})O_2$ delivers its capacity between 2.5–4.6 V in two discrete stages: ~50% capacity between 4–3.5 V ($Ni^{2+/4+}$ redox) and ~50% between 3.0–2.5 V ($Mn^{3+/4+}$ redox). Cyclic voltammetry also showed qualitative and quantitative differences in the redox behavior of $Li_{2/3}(Ni_{1/3}Mn_{2/3})O_2$ and $Li_{(2/3)+x}(Ni_{1/3}Mn_{2/3})O_2$.[17]

Similarly, $Li_{(2/3)+x}(Co_{0.15}Mn_{0.85})O_2$ shows an improved first-extraction capacity (250 mA h g^{-1}; 5 mA g^{-1}; 2.5–4.6 V *vs.* Li) as compared to 150 mA h g^{-1} for $Li_{2/3}(Co_{0.15}Mn_{0.85})O_2$ and a reversible capacity of ~180 mA h g^{-1} is observed (Fig. 2b).

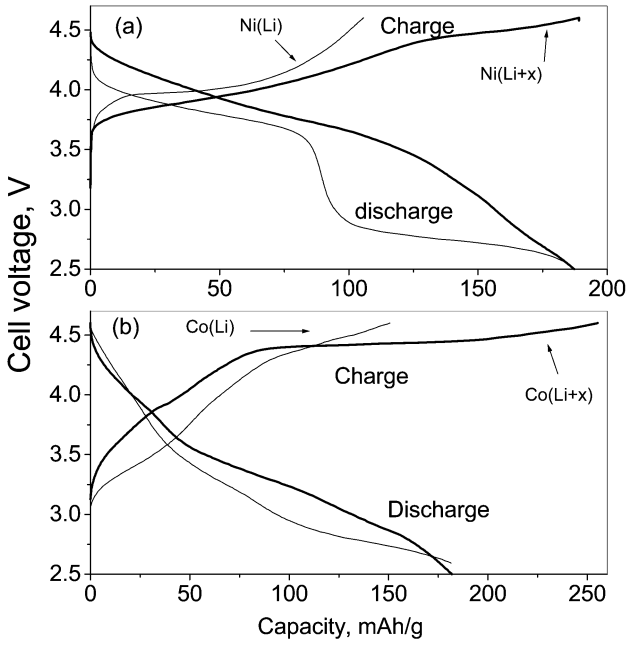

Fig. 2 Voltage *vs.* cathodic capacity profiles at ambient temperature between 2.5–4.6 V for the first-charge and first-discharge cycle. (a) $Li_{2/3}(Ni_{1/3}Mn_{2/3})O_2$ (Ni(Li)) and $Li_{(2/3)+x}(Ni_{1/3}Mn_{2/3})O_2$ (Ni(Li+x)) at 10 mA g^{-1}. (b) $Li_{2/3}(Co_{0.15}Mn_{0.85})O_2$ (Co(Li)) and $Li_{(2/3)+x}(Co_{0.15}Mn_{0.85})O_2$ (Co(Li+x)) at ~5 mA g^{-1}.

The value of the first-extraction-capacity obtained at low current charging is in accord with the stoichiometry of the compound (150 mA h g^{-1} corresponding to ~0.5 Li and 250 mA h g^{-1} corresponding to 0.85 Li), and the Co ion is assumed to be electrochemically inactive in the voltage region.

3.3 XPS of $A_{(2/3)+x}(Ni_{1/3}Mn_{2/3})O_2$ and $A_{(2/3)+x}(Co_{0.15}Mn_{0.85})O_2$; A = Li, Na; $x = 0, \sim\frac{1}{3}$

XPS is a useful non-destructive technique for studying the chemical state of elements, particularly the non-equivalence of atoms resulting from differences in formal oxidation state, ionic environment and lattice site in a compound.[21] A change in the chemical environment and oxidation state of an element can cause small changes in its BE and this has been used for assignment of the oxidation states of elements in oxide cathodes.[22–30]

Fig. 3 shows the Mn $2p_{3/2}$ and Ni $2p_{3/2}$ XPS core level spectra for $Na_{2/3}(Ni_{1/3}Mn_{2/3})O_2$, $Li_{2/3}(Ni_{1/3}Mn_{2/3})O_2$ and $Li_{(2/3)+x}(Ni_{1/3}Mn_{2/3})O_2$. The Mn ions in $Na_{2/3}(Ni_{1/3}Mn_{2/3})O_2$ and $Li_{2/3}(Ni_{1/3}Mn_{2/3})O_2$ are supposed to be in the 4+ oxidation state as per the electrochemical results and stoichiometry.[4,17,18] However, curve fitting of the spectra of the above two compounds gives two peaks. Comparing the BEs with the values reported for different Mn-containing compounds,[7,19,22–26] the intense peak centered at 642–643 eV corresponds to Mn^{4+} and the other peak at 641–642 eV corresponds to Mn^{3+} (Table 1 and Figs. 3a and b). The Mn $2p_{3/2}$ spectra of $Li_{(2/3)+x}(Ni_{1/3}Mn_{2/3})O_2$ can also be fitted to two peaks with nearly equal intensities (Fig. 3c). The peak at 643.1 eV can be assigned to Mn^{4+} and the one at 641.8 eV to Mn^{3+}. The slightly higher BEs observed for Mn^{3+} and Mn^{4+} ions in $Li_{(2/3)+x}(Ni_{1/3}Mn_{2/3})O_2$ could be due to stronger Mn–O bonds as evidenced from the smaller *c*-lattice parameter (9.91 Å in $Li_{(2/3)+x}(Ni_{1/3}Mn_{2/3})O_2$ *vs.* 10.06 Å in $Li_{2/3}(Ni_{1/3}Mn_{2/3})O_2$[17,18]) and/or due to a change in the chemical environment of the Mn ions due to the extra Li ($x = \frac{1}{3}$) in the lattice.

The Ni $2p_{3/2}$ XPS spectra show characteristic satellite peaks with a BE of ~861 eV (Fig. 3d–f). Such satellite peaks are the result of multiple splitting in the energy levels of Ni ions in oxides.[7,27,28,31] The curve fitting for the Ni $2p_{3/2}$ spectra of $Na_{2/3}(Ni_{1/3}Mn_{2/3})O_2$, $Li_{2/3}(Ni_{1/3}Mn_{2/3})O_2$ and $Li_{(2/3)+x}(Ni_{1/3}Mn_{2/3})O_2$ gives two BE values in each case. The high intensity peaks correspond to a BE of ~854 eV which are attributed to Ni^{2+} ions and the less prominent peak at ~856 eV corresponds to Ni^{3+} ions (Table 1). The BE value for Ni^{3+} is slightly higher (by 0.5 eV) than that reported for other Ni oxides.[7,28–30] This could be due to the P2 and O2 structures adopted by the compounds described herein.

Thus, the XPS results show that the predominant oxidation states of Ni and Mn ions in $Na_{2/3}(Ni_{1/3}Mn_{2/3})O_2$ and $Li_{2/3}(Ni_{1/3}Mn_{2/3})O_2$ are 2+ and 4+ respectively, and to a first approximation, the chemical formula can be written as shown in Table 1. The minor contribution of Ni^{3+} and Mn^{3+} is due to dynamic electron exchange between the Mn^{4+} and Ni^{2+} ion pairs, and from the relative peak intensities, rough estimates give the Mn^{3+}/Ni^{3+} content as 10–12% in both the above compounds. It may be mentioned that a similar dynamic ion equilibrium, $Ni^{4+} + Co^{3+} \leftrightarrow Ni^{3+} + Co^{4+}$ was reported in layered O3 $Li_x(Ni_{0.3}Co_{0.7})O_2$ at $x \sim 0.7$[32] and $Fe^{3+} + Ni^{4+} \leftrightarrow Fe^{4+} + Ni^{3+}$ in O3 $Li_x(Ni_{0.9}Fe_{0.1})O_2$, ($x < 0.9$).[33]

A rough estimate based on the relative intensities of the oxidation states of Mn in $Li_{(2/3)+x}(Ni_{1/3}Mn_{2/3})O_2$ from the XPS data (Fig. 3c) yields 56% Mn^{3+} and 44% Mn^{4+}. This compares well with the 50 : 50 ratio expected from the chemical formula, considering the fact that contribution from Mn^{3+} is enhanced in $Li_{(2/3)+x}(Ni_{1/3}Mn_{2/3})O_2$ due to the ion equilibrium (Figs. 3c and f). The amount of Ni^{3+} changed only slightly, from ~12% in $Li_{2/3}(Ni_{1/3}Mn_{2/3})O_2$ to ~15% for $Li_{(2/3)+x}(Ni_{1/3}Mn_{2/3})O_2$. This shows that incorporation of extra lithium is facilitated by

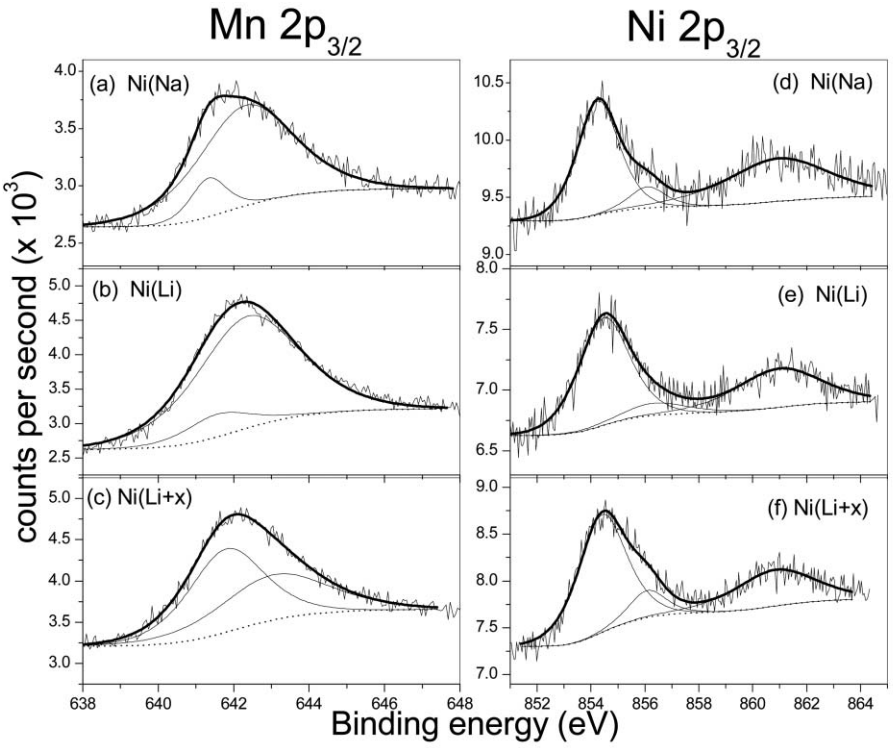

Fig. 3 XPS core-level spectra of Mn and Ni of $Na_{2/3}(Ni_{1/3}Mn_{2/3})O_2$ (Ni(Na)), $Li_{2/3}(Ni_{1/3}Mn_{2/3})O_2$ (Ni(Li)) and $Li_{(2/3)+x}(Ni_{1/3}Mn_{2/3})O_2$ (Ni(Li+x)). (a)–(c) Mn $2p_{3/2}$. (d)–(f) Ni $2p_{3/2}$. Curve fitting clearly shows two peaks for Mn and three peaks for Ni. The dotted line represents the Shirley-type background and the thick line represents the raw data.

the reduction of Mn^{4+} to Mn^{3+} in $Li_{(2/3)+x}(Ni_{1/3}Mn_{2/3})O_2$. It is worth mentioning that the higher cathodic first-extraction capacity observed in $Li_{(2/3)+x}(Ni_{1/3}Mn_{2/3})O_2$ as compared to $Li_{2/3}(Ni_{1/3}Mn_{2/3})O_2$ can be easily accounted for by the presence of more Mn^{3+} ions in the $Li_{(2/3)+x}(Ni_{1/3}Mn_{2/3})O_2$.

The Li 1s spectra are associated with the intense Mn 3p spectra in the 45–57 eV region (Fig. 4). Fitting of the Li 1s spectra gives a BE of 54.1 eV for $Li_{2/3}(Ni_{1/3}Mn_{2/3})O_2$ and 54.3 eV for $Li_{(2/3)+x}(Ni_{1/3}Mn_{2/3})O_2$; these values are in good agreement with the values reported in similar Li–oxide cathode materials.[7,19,22,29,30] Similar to the Mn $2p_{3/2}$ spectra, the Mn 3p spectra are also asymmetric and can be fitted to two peaks, assigned to Mn^{3+} and Mn^{4+}, as shown in Fig. 4 and Table 1. The BE values are in agreement with those reported for other Mn oxides.[26,30] The relative intensities of the fitted spectra of Mn^{3+} and Mn^{4+} (3p) in $Li_{2/3}(Ni_{1/3}Mn_{2/3})O_2$ and $Li_{(2/3)+x}(Ni_{1/3}Mn_{2/3})O_2$ match those of the Mn $2p_{3/2}$ spectra (Figs. 3 and 4).

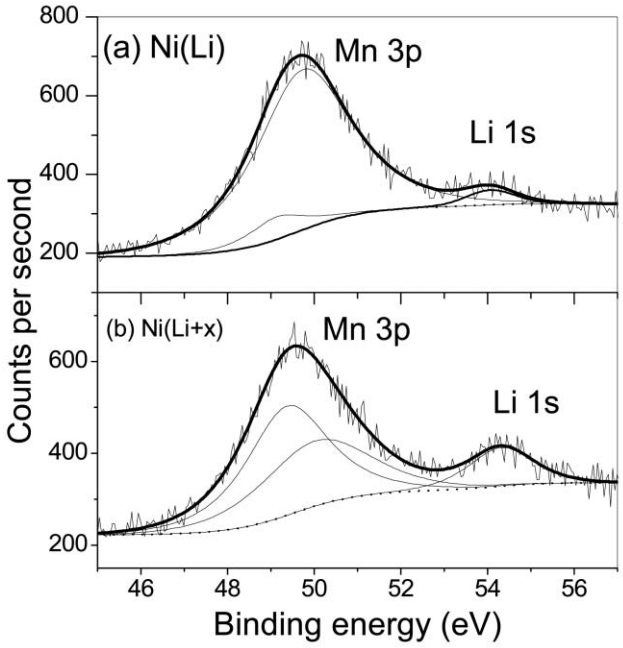

Fig. 4 Li 1s and Mn 3p XPS spectra of (a) $Li_{2/3}(Ni_{1/3}Mn_{2/3})O_2$ (Ni(Li)) and (b) $Li_{(2/3)+x}(Ni_{1/3}Mn_{2/3})O_2$ (Ni(Li+x)). Curve fitting clearly shows three peaks. The dotted line represents the Shirley-type background and the thick line represents the raw data.

The overlapping O 1s spectra commonly observed in oxide cathodes are a resultant contribution arising from Li-oxide and other (Li_2CO_3, LiOH) impurities on the surface in addition to the parent oxide.[7,19,22,29,30,34] The O 1s spectra of $Na_{2/3}(Ni_{1/3}Mn_{2/3})O_2$, $Li_{2/3}(Ni_{1/3}Mn_{2/3})O_2$ and $Li_{(2/3)+x}(Ni_{1/3}Mn_{2/3})O_2$ are shown in Fig. 5 and the BEs are given in Table 1. Similar to the assignments made for $Li(Ni_{1/2}Mn_{1/2})O_2$[30] and $Li(Ni_{1/3}Co_{1/3}Mn_{1/3})O_2$,[7] the peaks at ~529 eV are assigned to oxygen linked as Mn–O and those at ~531 eV to oxygen linked as Ni–O together with contributions from the Li-compound impurities.

The XPS spectra of $Na_{2/3}(Co_{0.15}Mn_{0.85})O_2$, $Li_{2/3}(Co_{0.15}Mn_{0.85})O_2$ and $Li_{(2/3)+x}(Co_{0.15}Mn_{0.85})O_2$ have been reported recently,[19] and the BEs of the Mn^{3+}, Mn^{4+} and Co^{3+} ions are given in Table 1. We re-analyzed the XPS data for 526–534 eV (O 1s) and 46–56 eV (Li 1s, Mn 3p). The Co $2p_{3/2}$ spectra for all the above compounds fit to a single peak with a BE of 780.0 ± 0.2 eV (Table 1). This value matches well the BE reported for Co^{3+} in $LiCoO_2$[9] and in $Li(Ni_{1/3}Co_{1/3}Mn_{1/3})O_2$[7] and is in agreement with the observation that Co in oxide cathodes adopts the 3+ oxidation state irrespective of the structure.[12,35] As can be seen from Table 1, the BE values for Mn^{3+} and Mn^{4+} in the Co-system and the respective values for the Ni-system compare well. The Li 1s spectra are associated with the Mn 3p signal in the 46–56 eV region in $Li_{2/3}(Co_{0.15}Mn_{0.85})O_2$ and $Li_{(2/3)+x}(Co_{0.15}Mn_{0.85})O_2$ (Fig. 6). The Li 1s BEs (Table 1) are in accord with those reported for similar Li–M–oxides.[7,19,22,29,30] The Mn 3p spectrum of $Li_{(2/3)+x}(Co_{0.15}Mn_{0.85})O_2$ fits to a single peak indicating the presence of

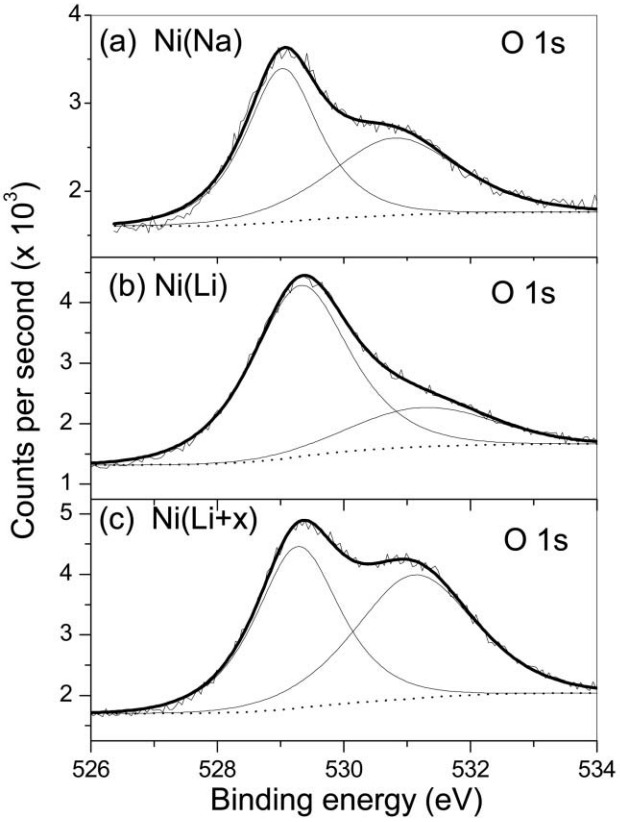

Fig. 5 O 1s XPS spectra of (a) $Na_{2/3}(Ni_{1/3}Mn_{2/3})O_2$ (Ni(Na)), (b) $Li_{2/3}$-$(Ni_{1/3}Mn_{2/3})O_2$ (Ni(Li)) and (c) $Li_{(2/3)+x}(Ni_{1/3}Mn_{2/3})O_2$ (Ni(Li+x)). Curve fitting clearly shows two peaks. The dotted line represents the Shirley-type background and the thick line represents the raw data.

only Mn^{3+} ions whereas for $Li_{2/3}(Co_{0.15}Mn_{0.85})O_2$, the asymmetric peak can be fitted to two peaks (Fig. 6), assigned to Mn^{3+} and Mn^{4+} ions as shown in Table 1. Fitting to the O 1s spectra (Fig. 7) show that two species contribute to these spectra. Following the arguments made earlier, peaks at ~529 eV can be assigned to oxygen linked as Mn–O in the

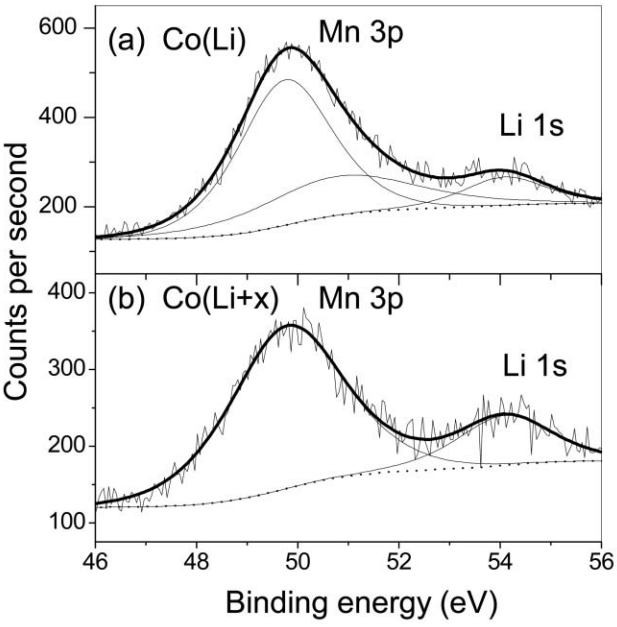

Fig. 6 Li 1s and Mn 3p XPS spectra of (a) $Li_{2/3}(Co_{0.15}Mn_{0.85})O_2$ (Co(Li)) and (b) $Li_{(2/3)+x}(Co_{0.15}Mn_{0.85})O_2$ (Co(Li+x)). Curve fitting clearly shows three peaks for the former and two for the latter. The dotted line represents the Shirley-type background and the thick line represents the raw data.

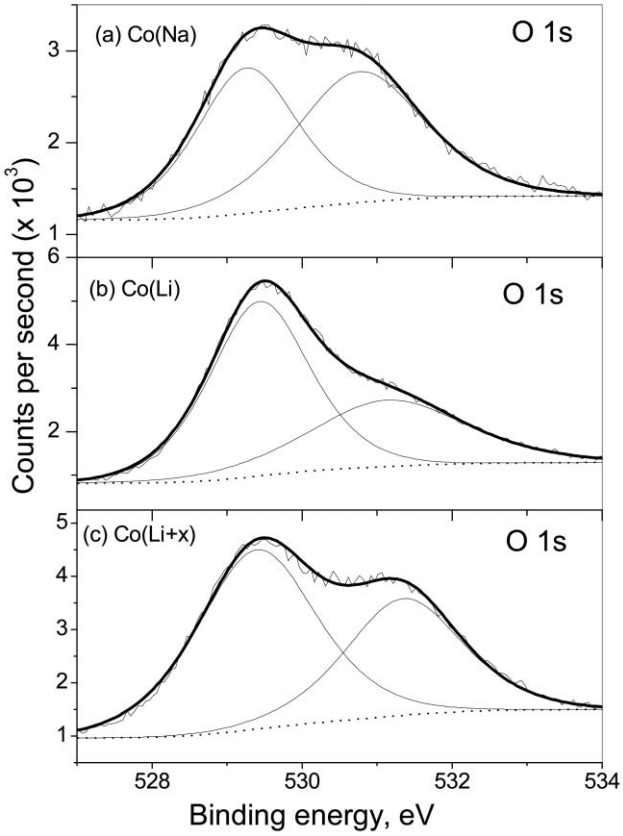

Fig. 7 O 1s XPS spectra of (a) $Na_{2/3}(Co_{0.15}Mn_{0.85})O_2$ (Co(Na)), (b) $Li_{2/3}$-$(Co_{0.15}Mn_{0.85})O_2$ (Co(Li)) and (c) $Li_{(2/3)+x}(Co_{0.15}Mn_{0.85})O_2$ (Co(Li+x)). Curve fitting clearly shows two peaks. The dotted line represents the Shirely-type background and the thick line represents the raw data.

compounds and those at ~531 eV have contributions from both Co–O linking and Li compound impurities.

3.4 FTIR spectra

The FTIR spectra of $Na_{2/3}(Ni_{1/3}Mn_{2/3})O_2$, $Li_{2/3}(Ni_{1/3}Mn_{2/3})O_2$ and $Li_{(2/3)+x}(Ni_{1/3}Mn_{2/3})O_2$ compounds along with those of the manganese spinel, $LiMn_2O_4$ and O3 $Li(Co_{0.1}Mn_{0.9})O_2$ (synthesized as described elsewhere[19,36]) are shown in Fig. 8. The IR

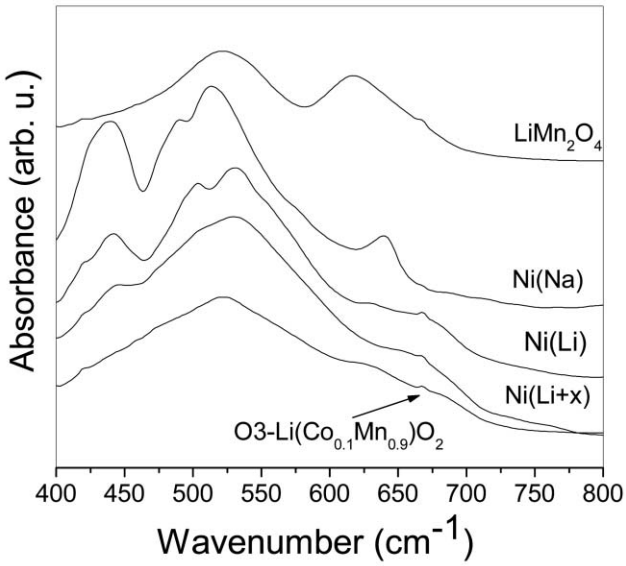

Fig. 8 FTIR spectra of compounds $Na_{2/3}(Ni_{1/3}Mn_{2/3})O_2$ (Ni(Na)), $Li_{2/3}$-$(Ni_{1/3}Mn_{2/3})O_2$ (Ni(Li)) and $Li_{(2/3)+x}(Ni_{1/3}Mn_{2/3})O_2$ (Ni(Li+x)). Spectra of spinel, $LiMn_2O_4$ and O3 $Li(Co_{0.1}Mn_{0.9})O_2$ are also shown.

spectra of the corresponding Co system of compounds have been reported earlier.[19] The band positions are accurate to ± 3 cm^{-1}. It is clear that the IR spectra of the layered compounds are distinctly different from that of the spinel, which shows two symmetric bands centered at 521 and 617 cm^{-1}, reflecting the high local symmetry of the cubic structure.[37,38] In the layered oxides, O3 $LiMO_2$ (M = Co, Ni) there are three IR active modes in the range 400–800 cm^{-1}, assigned to the stretching and bending vibrations of MO_6 octahedra.[8,19,39,40] In $LiCoO_2$ these bands are seen at 420, 540 and 600 cm^{-1}. A broad shoulder at 650 cm^{-1} is also observed. The spectrum of the P2 [$Na_{2/3}(Ni_{1/3}Mn_{2/3})O_2$] is similar to that reported for other layered oxides, with bands at around 440, 513 and 640 cm^{-1} and one shoulder peak at around 491 cm^{-1}. The positions of the bands in $Li_{2/3}(Ni_{1/3}Mn_{2/3})O_2$ shift to higher frequency compared to those of $Na_{2/3}(Ni_{1/3}Mn_{2/3})O_2$: the intense peak shifts to 531 cm^{-1}, the shoulder becomes a clear peak at 504 cm^{-1} and the peak at 640 cm^{-1} becomes a broad peak centred at $\sim$665 cm^{-1}. The shifting of the IR bands to higher wave number in $Li_{2/3}(Ni_{1/3}Mn_{2/3})O_2$ is expected from the difference in ionic mass and change in the lattice size. The XRD data show smaller crystallographic lattice parameters for $Li_{2/3}(Ni_{1/3}Mn_{2/3})O_2$ compared to those of $Na_{2/3}(Ni_{1/3}Mn_{2/3})O_2$,[17,18] and hence an increased bond strength can be expected in the former, in agreement with the IR results.

In the case of $Li_{(2/3)+x}(Ni_{1/3}Mn_{2/3})O_2$, the main absorption band is broadened with its center at 529 cm^{-1} and with shoulders at 446 and 665 cm^{-1}. This spectrum is similar to that of O3 $Li(Co_{0.1}Mn_{0.9})O_2$, shown in Fig. 8 for comparison. These similarities in the IR spectral features of O3 and O2 phases are expected since the cationic environment in both the compounds are identical. However, minor shifts in the main band and shoulder peaks are expected since the stacking sequence and orientation of the MO_2 and LiO_2 sheets are different (Fig. 1). Similar behaviour was noted in the IR spectra of $Na_{2/3}(Co_{0.15}Mn_{0.85})O_2$, $Li_{2/3}(Co_{0.15}Mn_{0.85})O_2$ and $Li_{(2/3)+x}(Co_{0.15}Mn_{0.85})O_2$.[19]

3.5 Magnetic susceptibility

Magnetic susceptibility studies on oxide cathodes have been reported.[22,35,41–48] The susceptibility (χ) and $1/\chi$ *vs.* T plots for the compounds presently being investigated are shown in Fig. 9. The Curie constant (C) and Weiss temperature (θ) were obtained by fitting the straight line portion of the $1/\chi(T)$ plots in the paramagnetic region, 180–300 K to the Curie–Weiss law, $\chi = C/(T - \theta)$. The θ and $\mu_{eff(exp)}$ values obtained are given in Table 1. Since the measurements were made only up to 300 K, these values are not very accurate though the general trends in the variation are reliable. The calculated $\mu_{eff(cal)} = (\Sigma n_i \mu_i^2)^{1/2}$ values, where n_i is the molar fraction of the magnetic ion and μ_i its moment given by $\mu_i = g[S_i(S_i + 1)]^{1/2}$ where $g = 2$ and S_i is the spin of the magnetic ion, are also given in Table 1. The susceptibility plots are typical of canted antiferromagnetic (AFM) materials: the susceptibility at high temperature has a negative θ value (AFM correlations) and is accompanied by ferromagnetic-like behavior at low temperature (<150 K). Taking into account the information obtained from the XPS data, the chemical formulae of $Li_{2/3}(Ni_{1/3}Mn_{2/3})O_2$ and $Li_{(2/3)+x}(Ni_{1/3}Mn_{2/3})O_2$ can respectively be written as $Li_{2/3}(Ni^{2+}_{0.29}Ni^{3+}_{0.04}Mn^{3+}_{0.08}Mn^{4+}_{0.59})O_2$ (12% each of Ni^{3+} and Mn^{3+}) and $Li_{1.0}(Ni^{2+}_{0.28}Ni^{3+}_{0.05}Mn^{3+}_{0.373}Mn^{4+}_{0.293})O_2$ (15% Ni^{3+} and 56% Mn^{3+}) due to ion equilibria. The respective $\mu_{eff(cal)}$ values are $3.63\mu_B$ and $3.97\mu_B$ assigning Ni^{3+} to the low-spin (LS) state. These are slightly higher than the calculated values using the stoichiometry given in Table 1. As can be seen, there is reasonable agreement between the $\mu_{eff(cal)}$ and the $\mu_{eff(exp)}$ values for the Ni-system of compounds (Table 1). Similar is the case with O2 $Li_{(2/3)+x}(Co_{0.15}Mn_{0.85})O_2$ if we assume Co^{3+} to be in the low-spin (LS) state. In other oxide cathodes like $LiCo^{3+}O_2$, $LiNi^{3+}O_2$, $Li(Co_{1-x}Ni_x)^{3+}O_2$, $Li(Co,Mn)O_4$, the Ni^{3+} and Co^{3+} ions have been found to be in the LS state.[5,6,32,44–46,49,50] On the other hand, the P2 $Na_{2/3}(Co_{0.15}Mn_{0.85})O_2$ and O2 $Li_{2/3}(Co_{0.15}Mn_{0.85})O_2$ have markedly lower $\mu_{eff(exp)}$ values. The reasons for this are not known at present and χ–T data at $T > 300$ K will be helpful in resolving

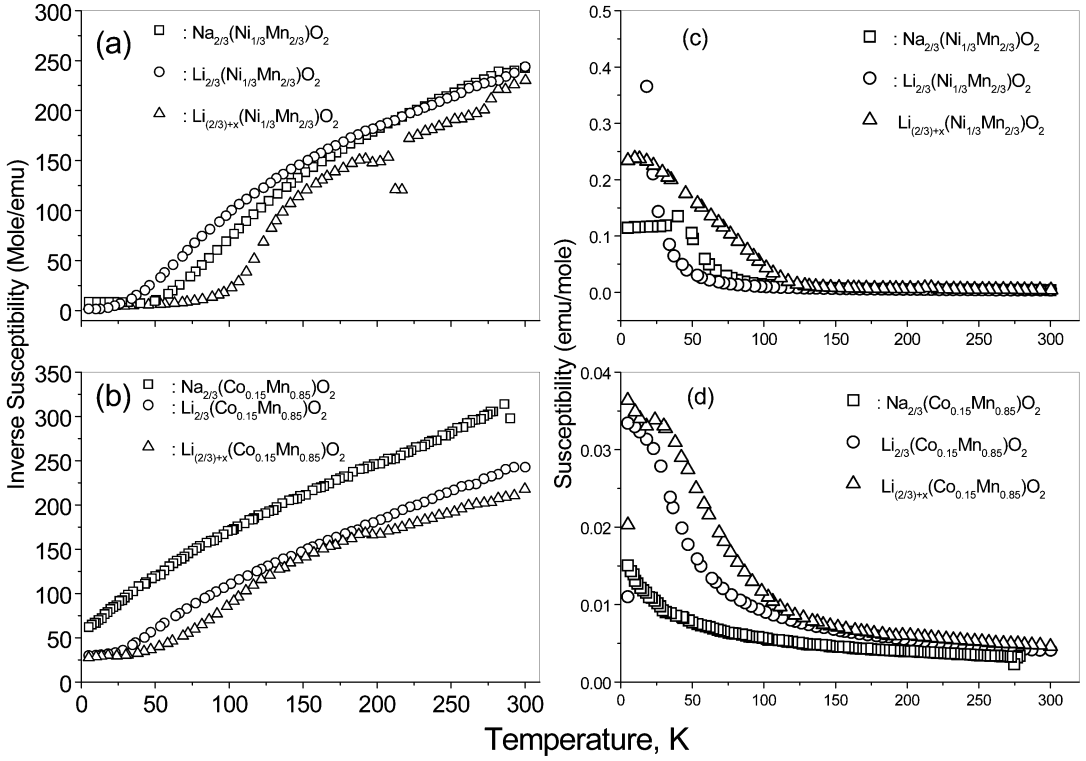

Fig. 9 Temperature variation of (a) and (b) the inverse molar susceptibility ($1/\chi$) and (c) and (d) the molar susceptibility (χ) for the P2- and O2-phase compounds.

the discrepancy. At $T < 100$ K, all the compounds display magnetic ordering. We can rule out ferromagnetism because at all values of T, the magnetization is much smaller than that expected from the alignment of all the spins. Similar ferrimagnetic or canted AFM behaviour has been reported for O3 $Li(Ni_{1-y}Co_y)O_2$, $y \leqslant 0.2$,[43] and for $Li(Ni_{1/2}Mn_{1/2})O_2$.[22]

The magnetic ordering in the O3- and O2-type layered compounds containing Mn and Ni ions in the metal layer can arise from uncompensated spins as a result of strong AFM interactions. In these oxides, two types of magnetic interaction exist within the metal layers:[46–48] (i) AFM Mn–Mn interactions between overlapping half-filled t_{2g} orbitals across a shared octahedral-site edge where both Mn^{3+} ($t_{2g}^3\ e_g^1$; high spin (HS)) and Mn^{4+} ($t_{2g}^3\ e_g^0$; HS) ions participate; (ii) 90° Mn–O–Mn interactions. In the latter case, if both ions are Mn^{4+}, which have empty e_g orbitals, the interaction will be ferromagnetic whereas if one or both the ions are Mn^{3+}, the interaction will be AFM.[42,45,48] In addition, for Ni^{2+} (or Ni^{3+}) AFM interactions predominate for both direct M–M and M–O–M (M = metal) interactions since these contain electrons in the e_g orbitals. Interlayer exchange also occurs through the 90° M–O–M pathway. This interaction is expected to be weak and AFM but it is pertinent in yielding three-dimensional character to the overall magnetic structure.

In the compounds P2 $Na_{2/3}(Ni_{1/3}Mn_{2/3})O_2$ and O2 $Li_{2/3}(Ni_{1/3}Mn_{2/3})O_2$, magnetic ordering may arise from uncompensated spins *via* Ni^{2+}–Mn^{4+} or Ni^{2+}–O–Mn^{4+} interactions whereas in $Li_{(2/3)+x}(Ni_{1/3}Mn_{2/3})O_2$, the Mn^{3+} ions will also participate to a significant extent (Table 1) to give additionally Ni^{2+}–Mn^{3+}- and Mn^{3+}–Mn^{4+}-type interactions. Further, minor amounts of Ni^{3+} (d^7 system; $t_{2g}^6\ e_g^1$; low spin (LS)) and Mn^{3+} (HS) present in $Na_{2/3}(Ni_{1/3}Mn_{2/3})O_2$ and $Li_{2/3}(Ni_{1/3}Mn_{2/3})O_2$ can also contribute to magnetic ordering. Ferrimagnetic behavior is evident from the hysteresis observed in the magnetization curve (Fig. 10) taken at 5 K for $Li_{(2/3)+x}(Ni_{1/3}Mn_{2/3})O_2$. This is definitely due to the presence of more Mn^{3+} in $Li_{(2/3)+x}(Ni_{1/3}Mn_{2/3})O_2$ as compared to that in $Li_{2/3}(Ni_{1/3}Mn_{2/3})O_2$.

P2 $Na_{2/3}(Co_{0.15}Mn_{0.85})O_2$ and O2 $Li_{2/3}(Co_{0.15}Mn_{0.85})O_2$ show predominantly AFM interactions with high negative values of θ (Fig. 9b and Table 1) and no clear magnetic ordering down to 5 K. This may be due to the fact that the Co^{3+} (d^6 system: $t_{2g}^6\ e_g^0$; LS) is expected to be diamagnetic. Though the Mn^{4+}–Mn^{3+} interactions are AFM, dilution due to the diamagnetic Co^{3+} ion must also be considered. Weak ferromagnetism in $Li_{2/3}(Co_{0.15}Mn_{0.85})O_2$ is also evident from the hysteresis loop shown in Fig. 10, which shows no magnetic saturation at 5 K. We also note that the θ value for $Na_{2/3}(Co_{0.15}Mn_{0.85})O_2$ is lower than that of $Li_{2/3}(Co_{0.15}Mn_{0.85})O_2$, which is opposite to the trend noted in $Na_{2/3}(Ni_{1/3}Mn_{2/3})O_2$ and $Li_{2/3}(Ni_{1/3}Mn_{2/3})O_2$. Compound $Li_{(2/3)+x}(Co_{0.15}Mn_{0.85})O_2$ shows pronounced ferrimagnetic behavior similar to that of $Li_{(2/3)+x}(Ni_{1/3}Mn_{2/3})O_2$ (Fig. 9b and Table 1). As $Li_{(2/3)+x}(Co_{0.15}Mn_{0.85})O_2$ has all its Mn ions in the 3+ oxidation state, the large negative θ in the paramagnetic region is understandable due to the strong Mn^{3+}–Mn^{3+} and Mn^{3+}–O–Mn^{3+} AFM interactions. However, the well-defined magnetic ordering below 25 K (Fig. 9b) was not expected. A plausible explanation for the magnetic ordering is the 'canting' of the Mn^{3+} spins below 100 K leading to weak ferromagnetism. Indeed, a canted-spin ferromagnetism below 100 K has been observed in the orthorhombically distorted layer compound, $LiMn^{3+}O_2$, by Greedan *et al.*[48]

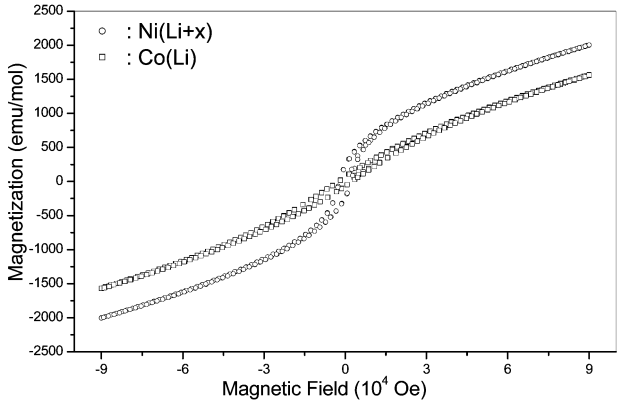

Fig. 10 Magnetization *vs.* magnetic field curves at 5 K for $Li_{(2/3)+x}(Ni_{1/3}Mn_{2/3})O_2$ (Ni(Li+x)) and $Li_{2/3}(Co_{0.15}Mn_{0.85})O_2$ (Co(Li)).

4 Conclusions

Layered O2-phase compounds have been prepared from the respective P2-phases with or without LiI treatment during ion exchange. The $Li_{(2/3)+x}(Ni_{1/3}Mn_{2/3})O_2$ shows an improved first-charge capacity compared to that of $Li_{2/3}(Ni_{1/3}Mn_{2/3})O_2$ when used as a cathode *vs.* Li metal in the voltage range, 2.5–4.6 V. Similarly, an increase in the first-charge capacity from 150 mA h g^{-1} in $Li_{2/3}(Co_{0.15}Mn_{0.85})O_2$ to 250 mA h g^{-1} in $Li_{(2/3)+x}(Co_{0.15}Mn_{0.85})O_2$ occurs. XPS studies have shown that the extra Li ($x \sim \frac{1}{3}$) incorporation is accompanied by the reduction of a corresponding amount of Mn^{4+} to Mn^{3+} ions in $Li_{(2/3)+x}(Ni_{1/3}Mn_{2/3})O_2$ and $Li_{(2/3)+x}(Co_{0.15}Mn_{0.85})O_2$ in agreement with the chemical analysis and electrochemical performance. The XPS BEs of the transition elements, Li and oxygen in the compounds obtained by the fitting of the raw spectra have been discussed. Minor changes in the IR band positions in the P2 and O2 phases as compared to those in the O3-phase are due to differences in the stacking sequences and orientation of the metal–oxygen octahedra. Magnetic susceptibility data show Curie–Weiss behavior at $T > 180$ K and weak ferrimagnetic ordering at $T < 100$ K), especially in $Li_{(2/3)+x}(Ni_{1/3}Mn_{2/3})O_2$ and $Li_{(2/3)+x}(Co_{0.15}Mn_{0.85})O_2$.

Acknowledgements

Thanks are due to Ms Liu Yan, Surface Science Laboratory, Department of Physics, NUS, Singapore, for help with the XPS measurements. KVR and SEL acknowledge the support of the New Jersey Commission on Higher Education for support.

References

1 A. Mendiboure, C. Delmas and P. Hagenmuller, *Mater. Res. Bull.*, 1984, **19**, 1383.
2 D. Carlier, I. Saadoune, L. Croguennec, M. Menetrier, E. Suard and C. Delmas, *Solid State Ionics*, 2001, **144**, 263.
3 J. M. Paulsen, C. L. Thomas and J. R. Dahn, *J. Electrochem. Soc.*, 1999, **146**, 3560.
4 J. M. Paulsen, C. L. Thomas and J. R. Dahn, *J. Electrochem. Soc.*, 2000, **147**, 861.
5 T. Ohzuku, A. Ueda, M. Nagayama, Y. Iwakoshi and H. Komori, *Electrochim. Acta*, 1993, **38**, 1159.
6 C. Delmas, M. Menetrier, L. Croguennec, I. Saadoune, A. Rougier, C. Pouillerie, G. Prado, M. Grune and L. Fournes, *Electrochim. Acta*, 1999, **45**, 243.
7 K. M. Shaju, G. V. Subba Rao and B. V. R. Chowdari, *Electrochim. Acta*, 2002, **48**, 145.
8 C. Julien, C. Letranchant, S. Rangan, M. Lemal, S. Ziolkiewicz, S. Castro-Garcia, L. El-Farh and M. Benkaddour, *Mater. Sci. Eng. B*, 2000, **76**, 145.
9 S. Madhavi, G. V. Subba Rao, B. V. R. Chowdari and S. F. Y. Li, *J. Electrochem. Soc.*, 2001, **148**, A1279.
10 A. R. Armstrong and P. G. Bruce, *Nature*, 1996, **381**, 499.
11 A. R. Armstrong, R. Gitzendanner, A. D. Robertson and P. G. Bruce, *Chem. Commun.*, 1998, 1833.
12 A. R. Armstrong, A. D. Robertson, R. Gitzendanner and P. G. Bruce, *J. Solid State Chem.*, 1999, **145**, 549.
13 J. M. Paulsen and J. R. Dahn, *J. Electrochem. Soc.*, 2000, **147**, 2478.

14 J. M. Paulsen, R. A. Donaberger and J. R. Dahn, *Chem. Mater.*, 2000, **12**, 2257.
15 Z. Lu and J. R. Dahn, *J. Electrochem. Soc.*, 2001, **148**, A710.
16 Z. Lu, R. A. Donaberger, C. L. Thomas and J. R. Dahn, *J. Electrochem. Soc.*, 2002, **149**, A1083.
17 K. M. Shaju, G. V. Subba Rao and B. V. R. Chowdari, *Electrochem. Commun.*, 2002, **4**, 633.
18 K. M. Shaju, G. V. Subba Rao and B. V. R. Chowdari, *J. Electrochem. Soc.*, 2003, **150**, A1.
19 K. M. Shaju, G. V. Subba Rao and B. V. R. Chowdari, *Solid State Ionics*, 2002, **152–153**, 69.
20 K. M. Shaju, G. V. Subba Rao and B. V. R. Chowdari, *Electrochim. Acta*, 2003, **48**, 2691.
21 *Practical Surface analysis, Vol.1-Auger and X-ray photoelectron spectroscopy*, eds. D. Briggs and M. P. Seah, John Wiley &Sons, New York, 1995.
22 M. E. Spahr, P. Novak, B. Schnyder, O. Haas and R. Nesper, *J. Electrochem. Soc.*, 1998, **145**, 1113.
23 K. M. Shaju, G. V. Subba Rao and B. V. R. Chowdari, *Solid State Ionics*, 2002, **148**, 343.
24 N. Treuil, C. Labrugere, M. Menetrier, J. Portier, G. Campet, A. Deshayes, J.-C. Frison, S.-J. Hwang, S.-W. Song and J.-H. Choy, *J. Phys. Chem. B*, 1999, **103**, 2100.
25 E. Regan, T. Groutso, J. B. Metson, R. Steiner, B. Ammundsen, D. Hassell and P. Pickering, *Surf. Interface Anal.*, 1999, **27**, 1064.
26 T. Eriksson, T. Gustafsson and J. O. Thomas, *Electrochem. Solid-State Lett.*, 2002, **5**, A35.
27 A. M. Andersson, D. P. Abraham, R. Haasch, S. MacLaren, J. Liu and K. Amine, *J. Electrochem. Soc.*, 2002, **149**, A1358.
28 K. Amine, H. Tukamoto, H. Yasuda and Y. Fujita, *J. Electrochem. Soc.*, 1996, **143**, 1607.
29 A. N. Mansour, *Surf. Sci. Spectra*, 1996, **3**, 279.
30 K. M. Shaju, G. V. Subba Rao and B. V. R. Chowdari, *Electrochim. Acta*, 2003, **48**, 1505.
31 A. F. Carley, S. D. Jackson, J. N. O'Shea and M. W. Roberts, *Surf. Sci.*, 1999, **440**, L868.
32 D. Carlier, M. Menetrier and C. Delmas, *J. Mater. Chem.*, 2001, **11**, 594.
33 G. Prado, A. Rougier, L. Fournes and C. Delmas, *J. Electrochem. Soc.*, 2000, **147**, 2880.
34 L. Hernan, J. Morales, L. Sanchez, J. Santos and E. R. Castellon, *Solid State Ionics*, 2000, **133**, 179.
35 P. Strobel, A. I. Palos, M. Anne and F. L. Cras, *J. Mater. Chem.*, 2000, **10**, 429.
36 K. M. Shaju, G. V. Subba Rao and B. V. R. Chowdari, *J. Mater. Chem.*, 2003, **13**, 106.
37 T. J. Richardson, S. J. Wen, K. A. Striebel, P. N. Ross, Jr., and E. J. Cairns, *Mater. Res. Bull.*, 1997, **32**, 609.
38 A. Rougier, K. A. Striebel, S. J. Wen, T. J. Richardson, R. P. Reade and E. J. Cairns, *Appl. Surf. Sci.*, 1998, **134**, 107.
39 W. Huang and R. Frech, *Solid State Ionics*, 1996, **86–88**, 395.
40 C. Julien, *Solid State Ionics*, 2000, **136–137**, 887.
41 J. N. Reimers, J. R. Dahn, J. E. Greedan, C. V. Stager, G. Liu, I. Davidson and U. V. Sacken, *J. Solid State Chem.*, 1993, **102**, 542.
42 C. Masquelier, M. Tabuchi, K. Ado, R. Kanno, Y. Kobayashi, Y. Maki, O. Nakamura and J. B. Goodenough, *J. Solid State Chem.*, 1996, **123**, 255.
43 I. Saadoune and C. Delmas, *J. Mater. Chem.*, 1996, **6**, 193.
44 A. Rougier, C. Delmas and G. Chouteau, *J. Phys. Chem. Solids*, 1996, **57**, 1101.
45 A. R. West, H. Kawai, H. Kageyama, M. Tabuchi, M. Nagata and H. Tukamoto, *J. Mater. Chem.*, 2001, **11**, 1662.
46 M. Takano, R. Kanno and T. Takeda, *Mater. Sci. Eng., B*, 1999, **63**, 6.
47 Y. Shimakawa, T. Numata and J. Tabuchi, *J. Solid State Chem.*, 1997, **131**, 138.
48 J. E. Greedan, N. P. Raju and I. J. Davidson, *J. Solid State Chem.*, 1997, **128**, 209.
49 L. A. Montoro, M. Abbate, E. C. Almedia and J. M. Rosolen, *Chem. Phys. Lett.*, 1999, **309**, 14.
50 V. R. Galakhov, V. V. Karelina, D. G. Kellerman, V. S. Gorshkov, N. A. Ovechkina and M. Neumann, *Phys. Solid State*, 2002, **44**, 266.